Published in final edited form as:
Environ Sci Technol. 2008 November 15; 42(22): 8528–8533.

Enhanced Formation of Oxidants from Bimetallic Nickel-Iron Nanoparticles in the Presence of Oxygen

Changha Lee and **David L. Sedlak***
Department of Civil and Environmental Engineering, 657 Davis Hall, University of California, Berkeley, California 94720

Abstract

Nanoparticulate zero-valent iron (nZVI) rapidly reacts with oxygen to produce strong oxidants, capable of transforming organic contaminants in water. However, the low yield of oxidants with respect to the iron added normally limits the application of this system. Bimetallic nickel-iron nanoparticles (nNi-Fe; i.e., Ni-Fe alloy and Ni-coated Fe nanoparticles) exhibited enhanced yields of oxidants compared to nZVI. nNi-Fe (Ni-Fe alloy nanoparticles with [Ni]/[Fe] = 0.28 and Ni-coated Fe nanoparticles with [Ni]/[Fe] = 0.035) produced approximately 40% and 85% higher yields of formaldehyde from the oxidation of methanol relative to nZVI at pH 4 and 7, respectively. Ni-coated Fe nanoparticles showed a higher efficiency for oxidant production relative to Ni-Fe alloy nanoparticles based on Ni content. Addition of Ni did not enhance the oxidation of 2-propanol or benzoic acid, indicating that Ni addition did not enhance hydroxyl radical formation. The enhancement in oxidant yield was observed over a pH range of 4 – 9. The enhanced production of oxidant by nNi-Fe appears to be attributable to two factors. First, the nNi-Fe surface is less reactive toward hydrogen peroxide (H_2O_2) than the nZVI surface, which favors the reaction of H_2O_2 with dissolved Fe(II) (the Fenton reaction). Second, the nNi-Fe surface promotes oxidant production from the oxidation of ferrous ion by oxygen at neutral pH values.

Introduction

The corrosion of zero-valent iron (ZVI or Fe^0) by oxygen (O_2) produces strong oxidants capable of transforming recalcitrant contaminants, providing a new approach for the oxidative treatment of contaminated soil and water. Recent studies have demonstrated the oxidation of aromatic compounds, chelating agents, and As(III) by the ZVI/O_2 system (1–3). Nanoparticulate zero-valent iron (nZVI) also produces oxidants upon exposure to O_2 (4,5). Relative to granular iron, nZVI shows not only increased reactivity due to its higher surface area, but also improved mobility, which is potentially applicable to *in situ* remediation by direct injection into the subsurface (6,7). The mechanism through which the ZVI/O_2 system produces oxidants involves the two-electron oxidation of Fe^0 followed by the Fenton reaction. In the initial step, Fe^0 surfaces transfer two electrons to O_2 (reaction 1) to produce hydrogen peroxide (H_2O_2), which is either reduced to water by another two-electron transfer from Fe^0 (reaction 2;8,9), or is converted into an oxidant by reaction with Fe(II) (i.e., Fenton reaction; reaction 3). The identity of oxidant produced by reaction 3 is uncertain. Under acidic conditions, it appears to be hydroxyl radical ($^{\bullet}OH$), but at pH values above 5, a different species such as Fe (IV) (e.g., FeO^{2+}) may be formed (10–12).

$$Fe^0_{(s)} + O_2 \xrightarrow{2H^+} Fe^{2+} + H_2O_2 \quad (1)$$

*Corresponding author. Phone: +1-510-643-0256; Fax.: +1-510-642-7483; E-mail: sedlak@ce.berkeley.edu.

$$Fe^0_{(s)} + H_2O_2 \xrightarrow{2H^+} Fe^{2+} + 2H_2O_2 \quad (2)$$

$$Fe^{2+} + H_2O_2 \rightarrow Fe^{3+} + {}^{\bullet}OH + OH^- \quad \text{or} \quad Fe(IV)\,(FeO^{2+}) + H_2O \quad (3)$$

Under neutral pH conditions, Fe(II), the primary product of ZVI oxidation by O_2 (reactions 1 & 2), also produces H_2O_2 when it is oxidized by O_2 (reactions 4 & 5), which subsequently forms oxidants through the Fenton reaction (13, 14). The oxidation of Fe(II) by O_2 is mainly responsible for the production of oxidants in the ZVI/O_2 system at neutral pH values (12).

$$Fe(II) + O_2 \rightarrow Fe(III) + O_2^{\bullet -} \quad (4)$$

$$Fe(II) + O_2^{\bullet -} \xrightarrow{2H^+} Fe(III) + H_2O_2 \quad (5)$$

Although the ZVI/O_2 system provides a means of activating O_2 for contaminant oxidation, the applicability of this approach to treatment is limited by the low yields of oxidants. In the absence of added ligands or catalysts, less than 10% of the Fe^0 is converted into oxidants capable of transforming contaminants (12). The low efficiency of the system is mainly due to the loss of H_2O_2 through the four-electron transfer process (reactions 1 & 2) and the precipitation of iron oxides and hydroxides at neutral pH. Recent studies have shown that the efficiency of the ZVI/O_2 system can be improved by the addition of iron-complexing ligands (1,3,15) or polyoxometalate (16,17), but such additions may not always be feasible.

Introduction of nickel to nZVI may provide another means of increasing the yields of oxidants in the nZVI/O_2 system. Several previous investigators have demonstrated that bimetallic nickel-iron particles show a higher reactivity than nZVI in the reductive transformation of contaminants (18–21). However, little is known about the potential of bimetallic nickel-iron particles to produce oxidants. The objective of the present study was to quantify and compare oxidant yields from nZVI and bimetallic nickel-iron nanoparticle (nNi-Fe) in the presence of O_2, and to provide a mechanistic interpretation for the observations. For this purpose, nZVI and two types of nNi-Fe (i.e., Ni-Fe alloy and Ni-coated Fe nanoparticles) were synthesized, and a series of experiments was carried out with compounds that are known to react with $^{\bullet}OH$ or Fe(IV).

Materials and Methods

Reagents

All chemicals except for 2,4-dinitrophenyl hydrazine (DNPH) were of reagent grade and were used without further purification. DNPH was recrystallized three times from acetonitrile prior to use. All solutions were prepared using 18 MΩ Milli-Q water from a Millipore system. The stock suspensions of nZVI and nNi-Fe were prepared daily. 50 mM Fe(II) stock solution was also prepared daily by dissolving ferrous sulfate in 0.1 mM HCl solution.

Synthesis of Nanoparticles

nZVI was synthesized by aqueous-phase reduction of ferrous sulfate through the dropwise addition of sodium borohydride solution as described previously (6,22). The same method was used to synthesize the Ni-Fe alloy nanoparticles with a mixture of ferrous sulfate and nickel (II) sulfate solutions as described previously (18). Ni-coated Fe nanoparticles were synthesized by a similar method to the procedure employed for production of Pd-coated Fe nanoparticles described by Wang and Zhang (23). The nZVI suspension was prepared first by aqueous-phase reduction of ferrous sulfate, followed immediately by addition of a nickel sulfate solution to form a Ni layer on the nZVI surface. Nanoparticles with different Ni content were synthesized

with both methods by varying the ratios of iron and nickel used in the synthesis procedure (i.e., [Ni(II)]/[Fe(II)] = 0.01, 0.05, and 0.1 for the Ni-Fe alloy nanoparticles, [Ni(II)]/[Fe(II)] = 0.1, 0.3, and 0.5 for the Ni-coated Fe nanoparticles). The freshly obtained suspensions of nZVI and nNi-Fe were washed three times with 10^{-4} N HCl solution by repeated centrifugation (4 min at 7000 rpm) and resuspension. The Fe and Ni content of the nanoparticles were determined by analyzing Fe and Ni ions completely dissolved from an acidified aliquot of nanoparticle stock suspension using a graphite furnace atomic absorption spectrometer (Perkin-Elmer 3300). The morphology of the nNi-Fe nanoparticles (Figure 1), measured with a FEI Tecnai 12 transmission electron microscope (TEM) at 120 kV, was similar to that of nZVI analyzed in a previous study (22). The Ni-coated Fe nanoparticles (Figures 1b) exhibited a similar range of primary particle size distribution to the Ni-Fe alloy nanoparticles (Figures 1a). However, they tended to disperse better than the Ni-Fe alloy nanoparticles. More TEM images of the Ni-Fe alloy and the Ni-coated Fe nanoparticles are provided in Supporting Information, Figures S1 & S2. The N_2-BET surface areas of nZVI, Ni-Fe alloy ([Ni]/[Fe] = 0.28), and Ni-coated Fe ([Ni]/[Fe] = 0.035) nanoparticles were determined as 34.5, 32.1, and 38.8 m^2/g, respectively.

Measurement of Oxidant Yields Using Probe Compounds

Methanol (CH_3OH) was used as a probe compounds for detecting oxidants in most experiments. 2-propanol, and benzoic acid ($pK_a = 4.2$) were also used in several experiments because they react with $^{\bullet}OH$ but not the oxidants produced by the Fenton reaction at neutral pH values (12). An excess of probe compounds (i.e., 200 mM methanol, 200 mM 2-propanol, and 10 mM benzoic acid) was employed to ensure that all of the oxidants were scavenged. Details regarding the selection of probe compounds and the analytical methods for their oxidation products are described elsewhere (12). The concentration of nZVI and nNi-Fe added was typically 100 μM expressed as Fe. All of the nanoparticles dissolved completely within 180 min under air saturation (open to the atmosphere; $[O_2]_0 = 0.25$ mM). In the absence of O_2, Fe(II) release from nZVI and nNi-Fe due to water reduction was negligible relative to that by the reaction with O_2 over the pH range of interest (i.e., pH > 2.9) (Supporting Information, Figure S3). The presence of 0.1 mM dissolved Ni(II) did not affect the oxidant formation from nZVI (Supporting Information, Figure S4).

Experimental Setup and Procedure

All experiments were performed at room temperature (20 ± 2°C) in 50 mL of reaction solution. For experiments conducted under acidic conditions (i.e., pH < 3), the solution pH was adjusted using 1 N HCl. For these experiments, the pH varied by less than 0.2 units during the reaction. Sodium acetate (1 mM) was used as a buffer for pH 4.0 – 4.5. The pH of neutral and alkaline solutions was buffered with 1 mM piperazine-N,N′-bis(ethanesulfonic acid) (PIPES) for pH 6 – 7 (24) or 2 mM borate for pH 8 – 10. Most experiments were performed with the reactor open to the atmosphere. As a result, the solutions contained carbonate ion that partitioned into the solutions from the atmosphere.

The experiments were initiated by adding an aliquot of freshly prepared nZVI or nNi-Fe stock suspensions to a pH-adjusted solution. Samples were withdrawn at predetermined timed intervals and filtered immediately through a 0.22-μm nylon filter. In experiments conducted under deaerated conditions, ultra-pure argon gas was bubbled through the solutions with a needle-type diffuser for 30 min prior to initiation of the reaction and during the entire experiment. Most of experiments were carried out in triplicate, and average values and the standard deviations are presented.

Analytical Methods

HCHO and acetone (i.e., the oxidized products of methanol and 2-propanol, respectively) were analyzed by HPLC and UV absorbance detection at 350 nm after DNPH derivatization (25).

Para-hydroxybenzoic acid (i.e., one of the oxidation products of benzoic acid) was analyzed using HPLC with UV detection at 270 nm. Separation was performed on a Waters Symmetry C18 column (150 mm × 4.6 mm, 5 μm), using water with 10 mM nitric acid and acetonitrile as the eluent, at a flow rate of 1.0 mL min^{-1}. Analyses of Fe(II) and total iron were carried out using 1,10–phenanthroline (26). For the analysis of total iron concentration, Fe(III) was reduced to Fe(II) with hydroxylamine hydrochloride prior to analysis.

Results

Oxidation of Methanol and Production of Fe(II)

The oxidation of CH_3OH to HCHO and the production of Fe(II) were studied at pH 4 and 7 in the nZVI/O_2 and the nNi-Fe/O_2 systems (Ni-Fe alloy with [Ni]/[Fe] = 0.28) (Figure 2). At pH 4, HCHO production in the nZVI/O_2 system was complete within 1 min, whereas the concentrations of HCHO in the nNi-Fe/O_2 systems slowly increased over 60 min (Figure 2a). The nZVI/O_2 system exhibited higher yields of HCHO than the nNi-Fe/O_2 system during the first 5 min of the reaction. However, after 10 min, the yield of HCHO in the nNi-Fe/O_2 system exceeded that observed in the nZVI/O_2 system. Fe(II) production followed similar kinetics to the HCHO production (Figure 2c). In the nZVI/O_2 system, Fe(II) was rapidly produced with its concentration plateauing after 3 min, whereas in the nNi-Fe/O_2 system, the concentration of Fe(II) gradually increased over 60 min.

At pH 7, HCHO production exhibited higher yields than those at pH 4 in both the nZVI/O_2 and the nNi-Fe/O_2 systems (Figure 2b). For both types of nanoparticles, the concentrations of HCHO gradually increased over 180 min. The nNi-Fe/O_2 system produced approximately twice as much HCHO than the nZVI/O_2 system. In both the systems, the concentrations of Fe (II) increased at almost same rates as was observed at pH 4 in the initial stages of the reaction. The initial rapid increase of Fe(II) was followed by gradual decrease due to the oxidation of Fe(II) by O_2 (Figure 2d). Fe(II) was completely consumed after 180 min in both the systems (data not shown).

Effects of Ni Content and Solution pH on the Oxidation of Methanol

The yield of HCHO was enhanced with increasing Ni content for both the Ni-Fe alloy and Ni-coated Fe nanoparticles (Figure 3). The effect of Ni addition was much more pronounced on the Ni-coated Fe nanoparticles relative to the Ni-Fe alloy nanoparticles. The Ni-coated Fe nanoparticle with [Ni]/[Fe] = 0.035 produced 18.7 μM HCHO, which is similar to the yield from the Ni-Fe alloy nanoparticle with [Ni]/[Fe] = 0.28 (i.e., 17.6 μM HCHO).

Enhanced yields of HCHO were observed for both types of nNi-Fe between pH 4 and 9 (Figure 4). The highest yields of HCHO were observed at around pH 7 in both the nZVI/O_2 and the nNi-Fe/O_2 systems, suggesting that same reaction mechanisms are involved in both the systems. It has been shown that the maximum yield of oxidant occurs around pH 7 in the nZVI/O_2 system due to increasing rates of Fe(II) oxidation by O_2 with pH and the decrease in iron availability due to iron precipitation at elevated pH values (12).

The addition of Ni to nZVI had the greatest effect on yields at neutral pH values (Figure 4) because the Fenton reaction predominantly produces Fe(IV) rather than $^{\bullet}OH$ under neutral pH conditions (10–12). The nNi-Fe/O_2 system did not significantly enhance the oxidation of 2-propanol or benzoic acid, both of which exhibit a low reactivity with Fe(IV) (10,11,27) (Supporting Information, Figure S5).

Reactivity of nZVI and nNi-Fe with O_2 and H_2O_2

The kinetics of the reactions of nZVI and nNi-Fe with O_2 and H_2O_2 were investigated at pH 4 and 7 (Figure 5), with 100 μM 1,10–phenanthroline added in the solution to measure Fe(II) production in situ and to prevent the oxidation of Fe(II) to Fe(III). In the presence of 0.25 mM O_2 (Figure 5a), the rates of Fe(II) release followed pseudo first-order kinetics, and showed no pH dependence for both nZVI and nNi-Fe. The apparent rate constants for release of Fe(II) from nZVI ($2.0 \times 10^{-2} \pm 6.4 \times 10^{-4}$ s^{-1}) were approximately an order of magnitude higher than those of nNi-Fe ($1.8 \times 10^{-3} \pm 7.0 \times 10^{-5}$ s^{-1}). In the presence of 1 mM H_2O_2 (Figure 5b), the rates of Fe(II) release decreased as the reactions proceeded, and did not follow pseudo first-order kinetics. As was the case for O_2, the reactions of nZVI were much faster than those of nNi-Fe. The dissolution of iron from nZVI and nNi-Fe in the absence of O_2 or H_2O_2 (due to water reduction) was negligible at both pH 4 & 7 (data not shown).

Effect of Fe(II) Addition on Methanol Oxidation by nZVI and nNi-Fe

Experiments were performed with addition of 0 – 150 μM Fe(II) to solutions containing 100 μM nZVI or nNi-Fe at pH 7 (Figure 6), to assess the effect of Fe(II) oxidation by O_2 on HCHO formation by the nZVI/O_2 and nNi-Fe/O_2 systems. Increases in HCHO production were linear with increases in Fe(II) added in both systems. However, the slope for the nNi-Fe/O_2 system ($9.6 \times 10^{-2} \pm 9.9 \times 10^{-3}$) was higher than that of the nZVI/O_2 system ($5.7 \times 10^{-2} \pm 4.7 \times 10^{-3}$).

Discussion

Oxidant Production from Fe^0

Oxidant production from the nZVI/O_2 and nNi-Fe/O_2 systems is explained by reactions 1 & 3 under acidic conditions and reactions 1 & 3 – 5 at higher pH values (i.e., pH > 6.5) (12). At pH 4, the concentration of Fe(II) observed after one hour accounted for 90 – 94% of the Fe^0 concentration initially added (Figure 2c) in both the systems, indicating that the oxidation of Fe(II) through the Fenton reaction (reaction 3) did not occur to a significant extent. This finding is consistent with the low yields of HCHO (<4 μM) relative to the concentration of Fe^0 added (100 μM) (Figure 2a), and indicates that reaction 2 is much more important than reaction 3. The 2:1 stoichiometry between Fe^0 oxidation and O_2 depletion reported in the previous study (12) also supports this explanation.

Under neutral pH conditions, Fe(II), the primary oxidation product of Fe^0 (from reactions 1 & 2), produces oxidants as it is oxidized by O_2 (reactions 3 – 5). Fe(II) oxidation by O_2 is the main source of oxidants in the ZVI/O_2 system at neutral pH values (12), and is responsible for increasing yields of HCHO between pH 5 and 7 (Figure 4). At pH 7, the concentration of Fe (II) increases initially by the oxidation of Fe^0, but gradually decreases as Fe(II) is oxidized by O_2 (Figure 2d). According to the stoichiometry of reactions 3 – 5, the theoretical yield of oxidant is 33% with respect to Fe(II); three moles of Fe(II) are oxidized to produce one mole of oxidant. However, the nZVI/O_2 and nNi-Fe/O_2 systems showed HCHO yields of 9.7% and 17.6% relative to the concentration of Fe^0 added at pH 7, respectively (Figure 2b). The lower-than-expected yields observed at neutral pH values are likely due to the precipitation of iron oxides and hydroxides on the nZVI surface, and the co-precipitation of Fe(II) and Fe(III) which limits Fe(II) availability (12).

Although they have the same reaction mechanism (reactions 1 – 5), the nNi-Fe/O_2 system exhibits higher oxidant production than the nZVI/O_2 system (Figure 2). The increased yield of HCHO is related to the effect of Ni on the kinetics of surface reactions (reactions 1 & 2). When compared on the basis of Ni content, the higher efficiency of Ni-coated Fe nanoparticles relative to Ni-Fe alloy nanoparticles (Figure 3) suggests that surface-mediated reactions play

a key role in the oxidant production in the nNi-Fe/O_2 system. nNi-Fe released Fe(II) more slowly because it exhibited a much lower reactivity with O_2 and H_2O_2 than nZVI (Figure 5) due to the oxidation resistance of nickel ($E_H^0[Fe^{2+}/Fe^0]$ = −0.447 V; $E_H^0[Ni^{2+}/Ni^0]$ = −0.257 V; 28). As discussed in the following sections, the slow surface reactions of nNi-Fe (reactions 1 & 2) explain the higher overall oxidant production by nNi-Fe.

Kinetics of Oxidant Production from nNi-Fe

The difference in reactivity with O_2 between nZVI and nNi-Fe surfaces explains the slower production of HCHO in the nNi-Fe/O_2 system compared to the nZVI/O_2 system at pH 4 (Figure 2a). The second-order rate constants for reaction 1 (k_1) can be calculated from the observed rates of Fe(II) release from nZVI and nNi-Fe under air saturation ($[O_2]_0$ = 0.25 mM) (Figure 5a). In the presence of O_2, Fe(II) release occurs via reaction 1 followed by reaction 2, and reaction 2 is much more important than reaction 3 ($k_2[Fe^0] \gg k_3[Fe(II)]$; Figure 2a). Therefore, its rate law is given by equation 6. The linearity of the pseudo first-order plots (Figure 5a) indicates that reaction 1 dominates the kinetics of iron dissolution (i.e., $k_1 \ll k_2$), enabling the use of a steady-state approximation for the concentration of H_2O_2 (equation 7).

$$-\frac{d[Fe^0]}{dt}=\frac{d[Fe(II)]}{dt}=k_1[Fe^0][O_2]+k_2[Fe^0][H_2O_2]=k_{obs}[Fe^0] \quad (6)$$

$$\frac{d[H_2O_2]}{dt}=k_1[Fe^0][O_2]-k_2[Fe^0][H_2O_2]\approx 0 \quad (7)$$

$$k_1=\frac{k_{obs}}{2[O_2]} \quad \text{(from equations 6\&7)} \quad (8)$$

Using equation 8, the k_1 values for nZVI and nNi-Fe were determined to be 40 ± 1.3 and 3.6 ± 0.14 M^{-1} s^{-1}, respectively. In both the the nZVI/O_2 and the nNi-Fe/O_2 systems, reaction 1 controls the kinetics for the oxidant production ($k_1 < k_3$ = 63 M^{-1} s^{-1} at pH < 3.5, 29; 2.3 × 10^4 M^{-1} s^{-1} at pH 7, 14). From the k_{obs} values (Figure 5a), the half lives of nZVI and nNi-Fe under air saturation are estimated to be 35 s and 6.4 min, respectively, which agree well with the observed rates of HCHO production (Figure 2a). The time-concentration profiles of Fe(II) in both the nZVI/O_2 and the nNi-Fe/O_2 systems (Figure 2c) showed the same trend as that observed for HCHO production.

At pH 7, HCHO production in the nZVI/O_2 system was also faster than that in the nNi-Fe/O_2 system during initial 3 min (inset of Figure 2b). However, after this initial period, both systems slowly produced HCHO through the oxidation of Fe(II) by O_2 in the bulk solution (reactions 4 & 5 followed by reaction 3). Reaction 4 is the rate-determining step for the oxidation of Fe(II), and its second-order rate constant is 1.7 M^{-1} s^{-1} at pH 7 (14). Assuming $[O_2]_0$ = 0.25 mM, the half life of Fe(II) at pH 7 is estimated to be 9 min (i.e., ln(2) / ($3k_4[O_2]$) = ln(2) / (3 × 1.7 × [2.5 × 10^{-4} M]) = 544 s), which is in reasonable agreement with the observed rates of HCHO production (Figure 2b).

Oxidant Production from Fe^0 Oxidation

At pH 4, the final yield of HCHO in the nNi-Fe/O_2 system (3.4 μM) was 42% higher than that in the nZVI/O_2 system (2.4 μM) (Figure 2a), indicating that the four-electron transfer process is less favored for nNi-Fe compared to nZVI. The four-electron oxidation (reactions 1 & 2) proceeds via the formation of adsorbed H_2O_2 on the Fe^0 surface (8, 9, 30), and the rate at which H_2O_2 desorbs from the Fe^0 surface determines the fraction of H_2O_2 that reacts with Fe(II) (i.e., reaction 3). The low reactivity of nNi-Fe surface with H_2O_2 (Figure 5b) increases the lifetime of adsorbed H_2O_2, which facilitates H_2O_2 release and increases the production of oxidant by

reaction 3. However, the measured increase in HCHO production in the nNi-Fe/O_2 system (42%; Figure 2a) was relatively small compared to the observed difference in reactivity with H_2O_2 between nZVI and nNi-Fe (approximately one order of magnitude; Figure 5b). The smaller-than-expected increase in HCHO production may be related to differences between H_2O_2 formed on the Fe^0 surface (reactions 1 & 2; Figure 2a) and H_2O_2 externally supplied in the bulk solution (the conditions employed in the experiments depicted in Figure 5b). Additional research would be required to resolve this issue.

Oxidant Production from Fe(II) Oxidation

The effect of Ni addition on oxidant production was more pronounced under neutral pH conditions (Figure 4). Increased oxidant production related to enhanced release of H_2O_2 from nNi-Fe can explain some of these increases because the reactivity of nNi-Fe with H_2O_2 is not significantly pH-dependent (Figure 5b). However, the large enhancement of the oxidant yield at pH 7 relative to that observed at pH 4 (i.e., 42% and 81% enhancement at pH 4 and 7, respectively; Figures 2a & 2b) must be related to Fe(II) oxidation by O_2. The oxidation of Fe (II) by O_2 produced almost identical yields of HCHO as the ZVI/O_2 system at pH values above 6.5 (Figure 4; 12,17), suggesting that the oxidation of Fe(II), the primary product of ZVI oxidation, is responsible for most of the oxidants produced by nZVI.

When Fe(II) is oxidized by O_2 in the absence of nanoparticles (filled circles in Figure 6), HCHO production increases as the concentration of Fe(II) added increases. For the first 50 μM of added Fe(II), approximately 9 μM of HCHO is produced, which corresponds to a little more than half of the theoretical maximum yield (i.e., 50 μM × 0.33 = 16.5 μM). As the amount of Fe(II) added increases, the percent yield of oxidant decreases because the co-precipitation of Fe(II) and Fe(III) (hydroxides or carbonates) is accelerated at a high concentration of Fe(II). When Fe(II) was added to solutions containing nanoparticles, different yields were observed (hollow symbols in Figure 6). For nNi-Fe, the yield was 9.6% whereas the slope for nZVI indicates a yield of 5.7%. The slow release of Fe(II) from nNi-Fe (Figures 2d, 5b) may have increased the oxidant yield by reducing the co-precipitation of Fe(II) and Fe(III).

Environmental Implications

Relative to nZVI/O_2, the nNi-Fe/O_2 system exhibits an increased yield of oxidants. However, the presence of Ni does not change the nature of the oxidants produced at different pH values. As a result, Ni addition does not increase the production of $^{\bullet}OH$, which is usually the objective of advanced oxidation processes used to treat organic contaminants. Therefore, the application of nNi-Fe is limited to situations where Fe(IV) is useful for treatment of contaminant, such as As(III) oxidation followed by coprecipitation or sorption on iron oxides (10,11).

The cost of nickel and the possible toxicity of the nickel ion released from nNi-Fe may be problematic for such applications. However, nickel is galvanically protected while iron is oxidized from nNi-Fe. For example, Schrick et al. have shown that the rate for the dissolution of nickel ion from nNi-Fe (≈ 30% Ni content) was three orders of magnitude lower than that of iron ion in the absence of O_2 (18). The potential concerns with cost and Ni release can be minimized by using Ni-coated Fe nanoparticles, which exhibited a considerable enhancement in the oxidant yield with a Ni content as low as 5% (Figure 3).

Supplementary Material

Refer to Web version on PubMed Central for supplementary material.

Acknowledgements

This research was supported by the US National Institute for Environmental Health Sciences (Grant P42 ES004705-19).

Literature Cited

1. Noradoun C, Engelmann M, McLauglin M, Hutcheson R, Breen K, Paszczynski A, Cheng IF. Destruction of chlorinated phenols by dioxygen activation under aqueous room temperature and pressure conditions. Ind Eng Chem Res 2003;42:5024–5030.
2. Leupin OX, Hug SJ, Badruzzaman ABM. Aesenic removal from Bangladesh tube well water with filter columns containing zerovalent iron filings and sand. Environ Sci Technol 2005;39:8032–8037. [PubMed: 16295871]
3. Englehardt J, Meeroof D, Echegoyen L, Deng Y, Raymo F, Shibata T. Oxidation of aqueous EDTA and associated organics and coprecipitation of inorganics by ambient iron-mediated aeration. Environ Sci Technol 2007;41:270–276. [PubMed: 17265958]
4. Joo SH, Feitz AJ, Waite TD. Oxidative degradation of the carbothiolate herbicide, molinate, using nanoscale zero-valent iron. Environ Sci Technol 2004;38:2242–2247. [PubMed: 15112830]
5. Joo SH, Feitz AJ, Sedlak DL, Waite TD. Quantification of the oxidizing capacity of nanoparticulate zero-valent iron. Environ Sci Technol 2005;39:1263–1268. [PubMed: 15787365]
6. Li L, Fan MH, Brown RC, Van Leeuwen JH, Wang JJ, Wang WH, Song YH, Zhang PY. Synthesis, properties, and environmental applications of nanoscale iron-based materials: A review. Crit Rev Environ Sci Technol 2006;36:405–431.
7. Hydutsky BW, Mack EJ, Beckerman BB, Skluzacek JM, Mallouk TE. Optimization of Nano- and Microiron Transport through Sand Columns Using Polyelectrolyte Mixtures. Environ Sci Technol 2007;41:6418–6424. [PubMed: 17948788]
8. Zecevic S, Drazic DM, Gojkovic S. Oxygen reduction on iron. Part III. An analysis of the rotating disk-ring electrode measurements in near neutral solutions. J Electroanal Chem 1989;265:179–193.
9. Zecevic S, Drazic DM, Gojkovic S. Oxygen reduction on iron. Part IV. The reduction of hydrogen peroxide as the intermediate in oxygen reduction reaction in alkaline solutions. Electrochimica Acta 1991;36:5–14.
10. Hug SJ, Canonica L, Wegelin M, Gechter D, von Gunten U. Solar oxidation and recmoval of arsenic at circumneutral pH in iron containing waters. Environ Sci Technol 2001;35:2114–2121. [PubMed: 11393995]
11. Hug SJ, Leupin O. Iron-catalyzed oxidation of arsenic(III) by oxygen and by hydrogen peroxide: pH-dependent formation of oxidant in the Fenton reaction. Environ Sci Technol 2003;37:2734–2742. [PubMed: 12854713]
12. Keenan CR, Sedlak DL. Factors affecting the yields of oxidants from the reaction of nanoparticulate zero-valent iron and oxygen. Environ Sci Technol 2008;42:1262–1267. [PubMed: 18351103]
13. Stumm W, Lee GF. Oxygenation of ferrous iron. Ind Eng Chem 1961;53:143–146.
14. King DW, Lounsbury HA, Millero FJ. Rates and mechanism of Fe(II) oxidation at nanomolar total iron concentrations. Environ Sci Technol 1995;29:818–824.
15. Keenan CR, Sedlak DL. Ligand-Enhanced Reactive Oxidant Generation by Nanoparticulate Zero-Valent Iron and Oxygen. Environ Sci Technol. 2008In press
16. Lee J, Kim J, Choi W. Oxidation on zerovalent iron promoted by polyoxometalate as an electron shuttle. Environ Sci Technol 2007;41:3335–3340. [PubMed: 17539546]
17. Lee C, Keenan CR, Sedlak DL. Polyoxometalate-enhanced oxidation of organic compounds by nanoparticulate zero-valent iron and ferrous ion in the presence of oxygen. Environ Sci Technol 2008;42:4921–4926. [PubMed: 18678027]
18. Schrick B, Blough JL, Jones AD, Mallouk TE. Hydrodechlorination of trichloroethylene to hydrocarbons using bimetallic nickel-iron nanoparticles. Chem Mater 2002;14:5140–5147.
19. Tee YH, Grulke E, Bhattacharyya D. Role of Ni/Fe Nanoparticle composition on the degradation of trichloroethylene from water. Ind Eng Chem Res 2005;44:7062–7070.

20. Gui L, Gillham RW, Odziemkowski MS. Reduction of *N*-nitrosodimethylamine with granular iron and nickel-enhanced iron. 1. Pathways and kinetics. Environ Sci Technol 2000;34:3489–3494.
21. Odziemkowski MS, Gui L, Gillham RW. Reduction of *N*-nitrosodimethylamine with granular iron and nickel-enhanced iron. 2. Mechanistic studies. Environ Sci Technol 2000;34:3495–3500.
22. Lee C, Kim JY, Lee WI, Nelson KL, Yoon J, Sedlak DL. Bactericidal effect of zero-valent iron nanoparticles on *Escherichia coli*. Environ Sci Technol 2008;42:4927–4933. [PubMed: 18678028]
23. Wang CB, Zhang WX. Synthesizing nanoscale iron particles for rapid and complete dechlorination of TCE and PCBs. Environ Sci Technol 1997;31:2154–2156.
24. Yu Q, Kandegedara A, Xu Y, Rorabacher DB. Avoiding interferences from Good's buffers: A contiguous series of noncomplexing tertiary amine buffers covering the entire range of pH 3-11. Analytical Biochem 1997;253:50–56.
25. Zhou X, Mopper K. Determination of photochemically produced hydroxyl radicals in seawater and freshwater. Mar Chem 1990;30:71–88.
26. Tamura H, Goto K, Yotsuyanagi T, Nagayama M. Spectrophotometric determination of iron(II) with 1,10-phenanthroline in the presence of large amounts of iron(III). Talanta 1974;21:314–318. [PubMed: 18961462]
27. Jacobsen F, Holcman J, Sehested K. Reactions of the ferryl ion with some compounds found in cloud water. Int J Chem Kinetics 1998;30:215–221.
28. Bard, AJ.; Parsons, R.; Jordan, J. Standard potentials in aqueous solution. Marcel Dekker, Inc.; New York, Basel: 1985.
29. Laat JD, Gallard H. Catalytic decomposition of hydrogen peroxide by Fe(III) in homogeneous aqueous solution: Mechanism and kinetic modeling. Environ Sci Technol 1999;33:2726–2732.
30. Jovancicevic V, Bockris JO'M. The mechanism of oxygen reduction on iron in neutral solutions. J Electrochem Soc 1986;133:1797–1807.

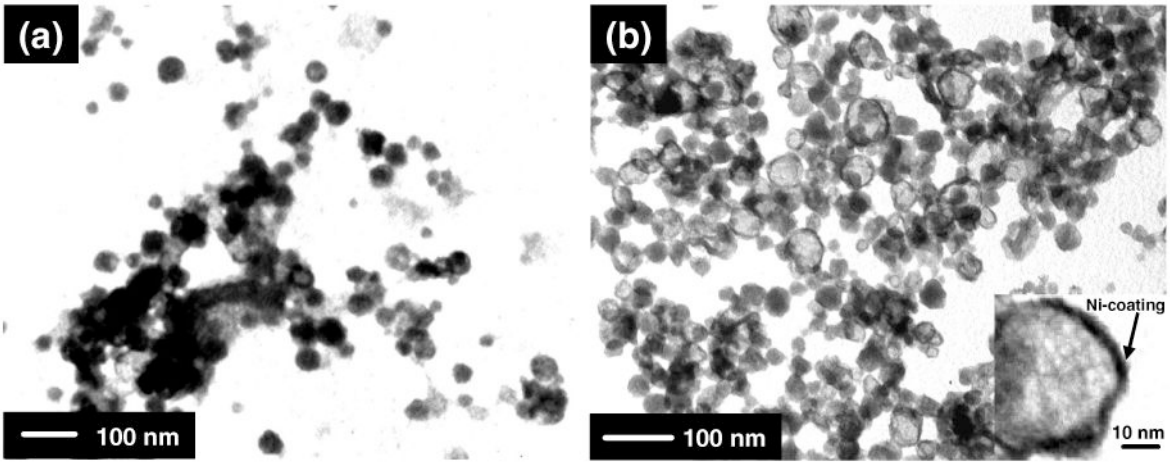

Figure 1.
Transmission electron microscopy images of synthesized bimetallic Ni-Fe nanoparticles (nNi-Fe), (a) Ni-Fe alloy ([Ni]/[Fe] = 0.28), (b) Ni-coated Fe ([Ni]/[Fe] = 0.035).

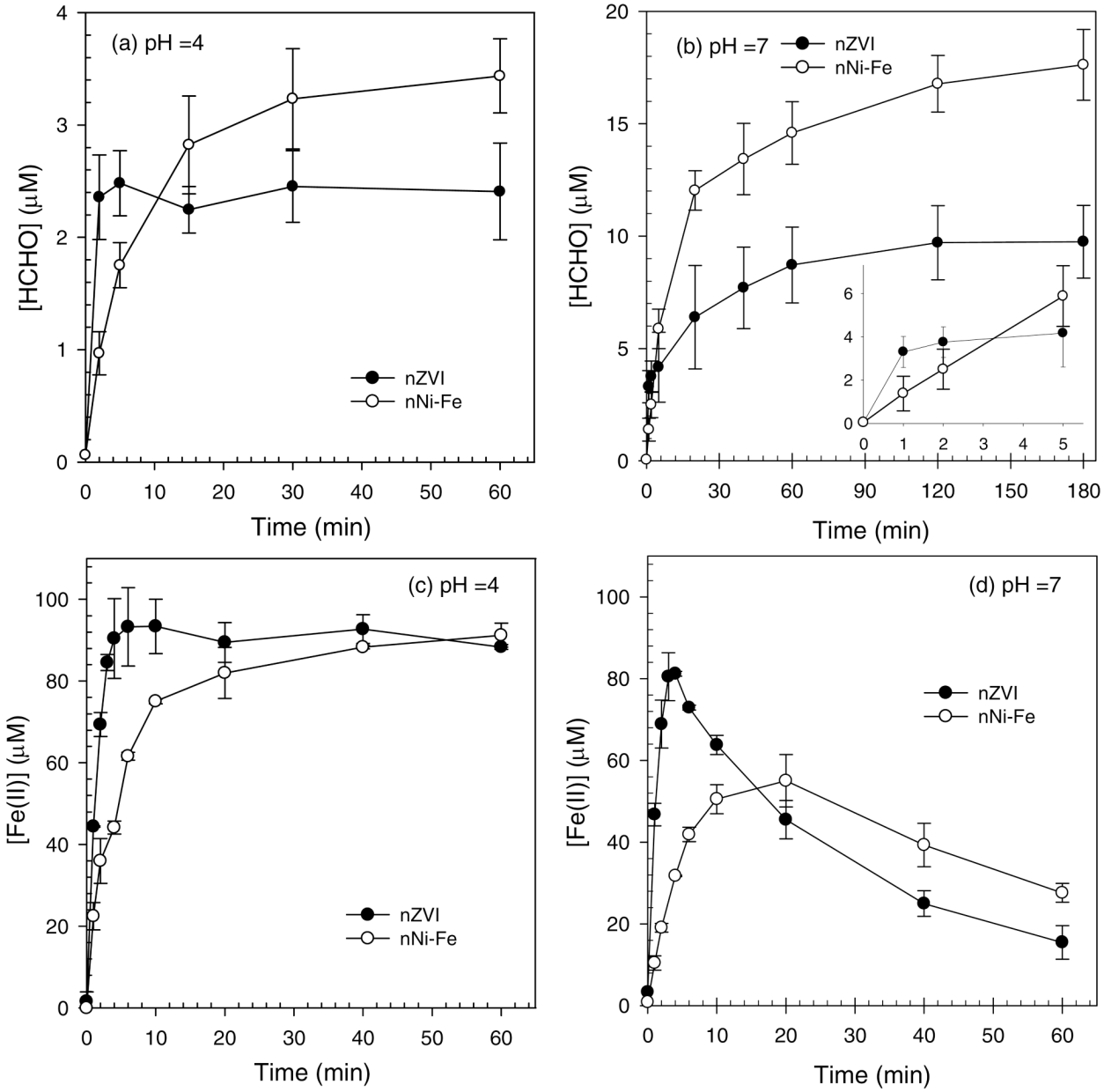

Figure 2.
Production of HCHO and Fe(II) from nZVI and nNi-Fe (Ni-Fe alloy nanoparticle, [Ni]/[Fe] = 0.28) as a function of time: $[CH_3OH]_0$ = 200 mM; $[Fe^0]_0$ = 100 μM.

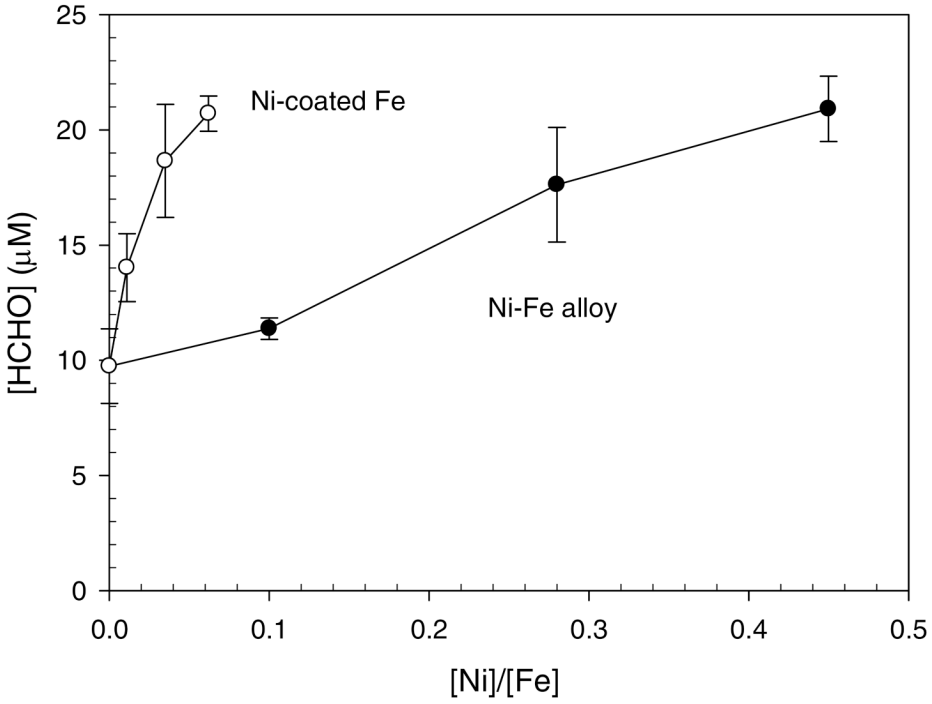

Figure 3.
HCHO production from nNi-Fe nanoparticles as a function of Ni content: $[CH_3OH]_0$ = 200 mM; $[Fe^0]_0$ = 100 μM; pH = 7.0, reaction time = 180 min.

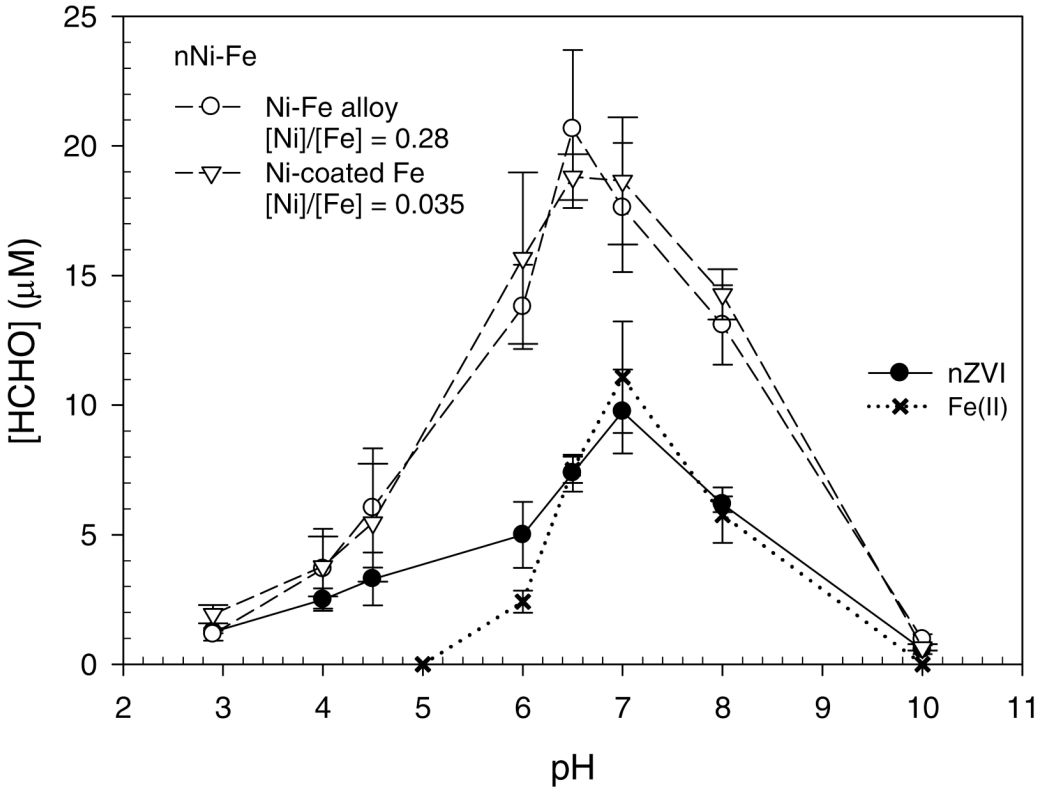

Figure 4.
HCHO production from nZVI, nNi-Fe, and Fe(II) as a function of pH: $[CH_3OH]_0$ = 200 mM; $[Fe^0]_0 = [Fe(II)]_0$ = 100 μM; reaction time = 180 min.

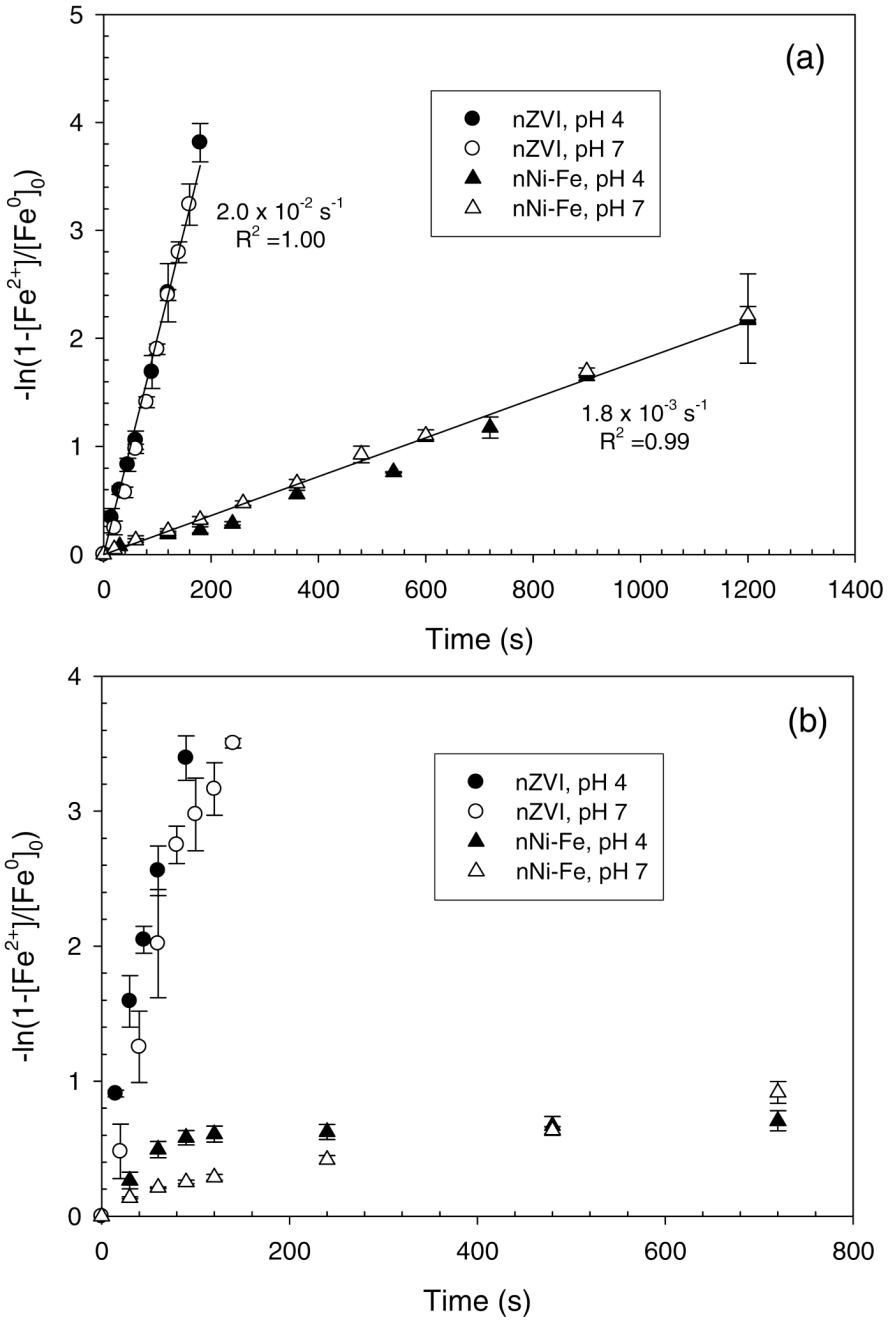

Figure 5.

Time-dependent iron dissolution from reactions of nZVI and nNi-Fe (Ni-Fe alloy nanoparticles, [Ni]/[Fe] = 0.28) with (a) O_2 and (b) H_2O_2: $[Fe^0]_0$ = 20 μM; [1,10-phenanthroline]$_0$ = 100 μM; (a) $[O_2]_0$ = 250 μM, air saturation; (b) $[H_2O_2]_0$ = 1.0 mM, argon saturation.

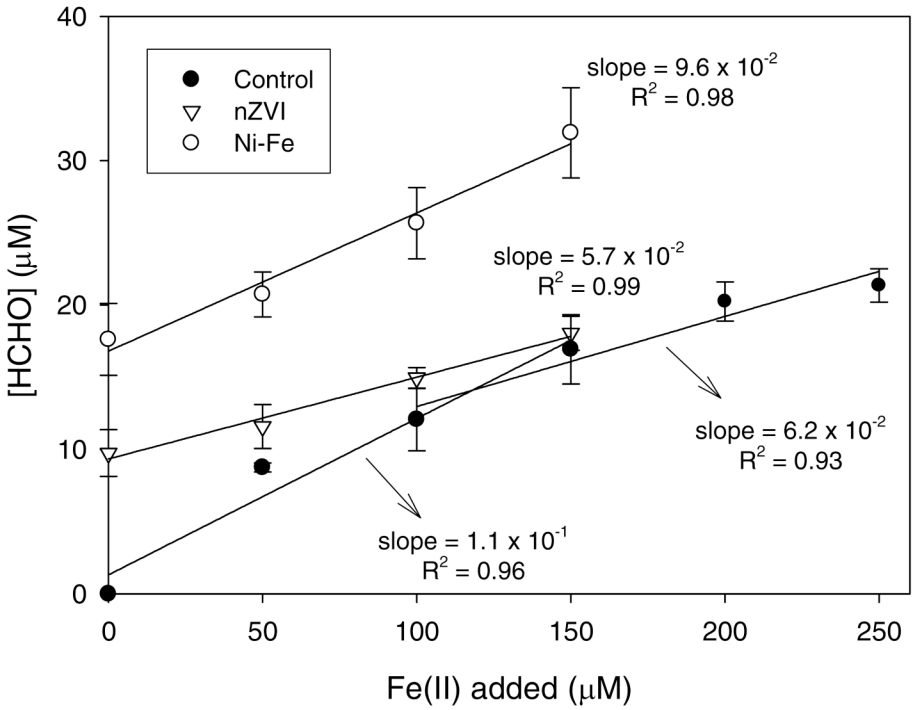

Figure 6.

HCHO production from Fe(II), nZVI with Fe(II) added, and nNi-Fe (Ni-Fe alloy nanoparticle, [Ni]/[Fe] = 0.28) with Fe(II) added: $[Fe(II)]_0 = [Fe^0]_0 = 100$ μM; $[CH_3OH]_0 = 200$ mM; pH = 7.0, reaction time = 180 min.